Mon. Not. R. Astron. Soc. **000**, 1–?? (2014) Printed 13 November 2016 (MN LATEX style file v2.2)

Stability boundaries of circumbinary planets in inclined orbits

Michael Hammer[1,2⋆], Diego J. Muñoz[1,3] and Dong Lai[1,4]
[1] *Center for Astrophysics and Planetary Science, Department of Astronomy, Cornell University, Ithaca, NY 14853, USA*
[2] *Department of Astronomy and Steward Observatory, University of Arizona, Tucson, AZ 85721, USA*
[3] *Physics Department, Technion - Israel Institute of Technology, Haifa, Israel 3200003*
[4] *Institute for Advanced Study, Princeton, NJ 08540, USA*

13 November 2016

ABSTRACT
We present parametric fits to the orbital stability boundaries for circumbinary planets over a parameter space spanning a wide range of different (i) binary mass ratios, (ii) binary eccentricities, and (iii) prograde planet inclinations over an integration time of 3×10^5 binary periods, a significant increment in the integration duration of previous studies. Each binary configuration features an inner region of unstable orbits, an outer region of stable orbits, and a meta-stable region in-between where orbits can be stable or unstable depending on their proximity to $n : 1$ mean motion resonances (MMRs). We characterize the inner limit of stability around a binary with a semi-major axis $a_{\rm crit}$ inside which all near circular orbits are unstable. Beyond $a_{\rm st}$, all orbits are stable throughout the integration. Values of $a_{\rm st}$ are typically $13 \pm 10\%$ larger than $a_{\rm crit}$. Binaries with equal mass ratios have slightly lower stability limits compared to those with low mass ratios, and the strongest dependence of both stability limits is on eccentricity. The dependences of both $a_{\rm crit}$ and $a_{\rm st}$ on inclination are very weak. For low inclinations $\leqslant 40^\circ$, the values of $a_{\rm crit}$ and $a_{\rm st}$ are largely identical to the respective values for coplanar orbits around the same binary. For non-equal mass binaries, we find regimes in which planets very distant from the binary can become unstable in the very long run, presumably evidencing dynamical instabilities aided by secular evolution.

Key words: star: planetary system – planets: dynamical evolution and stability

1 INTRODUCTION

The discovery of circumbinary planets (CBPs) by the *Kepler* mission (e.g. Doyle et al. 2011; Orosz et al. 2012; Welsh et al. 2012) has revealed the resilience of the planet formation process. Perhaps once a surprising discovery, CBPs have now been established as not an uncommon phenomenon. The ten currently known systems of this kind suggest a Neptune-size planet-bearing frequency that is comparable to that of single stars if coplanarity with the host stars is assumed (Fressin et al. 2013; Armstrong et al. 2014); however, if the distribution of planetary inclinations is instead isotropic, the planet-bearing frequency can increase dramatically (up to $\sim 50\%$ according to Armstrong et al. 2014).

To date, no CBPs have been found with misalignments greater than $\approx 4^\circ$ (Kostov et al. 2014). All currently known systems of *close-in* CBPs have been detected by the transit method around eclipsing binaries, which is strongly biased against misaligned planetary orbits (Schneider 1994; Martin & Triaud 2014; Kostov et al. 2014) . Detection strategies within the reach of current observational capabilities, such as long-baseline searches for precessing orbits that are in on-and-off transiting configurations (Kostov et al. 2014; Martin & Triaud 2015), transit detection across non-eclipsing binaries (Martin & Triaud 2015) and even planet-induced eclipse timing variations (Borkovits et al. 2003) have not been carried out systematically. Thus, the fraction of CBPs that are in inclined respect to their host stars is still unconstrained.

Although planetary orbits coplanar with the central binary are favored by the in-disc formation (and migration) scenario (as the parental discs themselves are thought to evolve into coplanarity, see e.g., Foucart & Lai 2013), observationally, the evidence against the existence of misaligned CBPs is far from conclusive given the inherent biases of the dominant detection method. The slight misalignment of Kepler-413b (Kostov et al. 2014), in addition to the suggestion that additional stellar companions might induce misalignment (Muñoz & Lai 2015; Martin & Triaud 2015; Hamers et al. 2016), opens the possibility for a yet unobserved population of misaligned planets. Showing that such inclined planets can exist in stable configurations –and could even be hiding in the *Kepler* data– would offer great promise for increasing the occurrence rate of CBPs, bringing us closer to understanding whether planet formation around binaries is fundamentally different from that around single stars.

Inclined CPBs can show richer dynamical behavior than coplanar ones. One crucial property of circumbinary dynamics is the minimum semi-major axis for which planets can be in a stable (long-lived) orbit. Interestingly, one of the most notable prop-

⋆ E-mail: mhammer@as.arizona.edu

erties of known CBPs is the propensity of these to lie very close to the semi-major axis below which long-term dynamical stability is not possible (e.g., Welsh et al. 2014). The proximity to this stability boundary, which can be parametrized as a function of the binary's orbital properties (Holman & Wiegert 1999), has been invoked as tentative evidence for disc-driven migration, which would bring planets right up to the circumbinary gas disc edge (with those that migrate further in getting simply ejected from the system). The dependence of this critical semi-major axis with planet inclination has not yet been fully explored (although, see Doolin & Blundell 2011). The tantalizing possibility of an undetected population of CBPs in a wide range of inclinations (brining up the planet occurrence rate significantly) underscores the importance of knowing the minimum allowed proximity to the binary, as it directly affects the likelihood of detection.

Parametrized stability criteria are of useful tool to quickly assess the plausibility or the expected life time of observed planetary systems. Usually, stability criteria vary according to the mass regime of interest, differing in functional form for circumbinary planets (henceforth HW99), planet pairs on close circular orbits (Wisdom 1980; Gladman 1993), hierarchical triples of comparable masses (Mardling & Aarseth 2001) or hierarchical planet pairs orbiting a single star (Petrovich 2015). Most of these criteria work best in coplanarity, having limited applicability at large mutual inclinations. In this paper, we address the relatively unexplored long-term stability of circumbinary orbits using direct N-body integrations, extending previous studies by exploring the dependence of the stability limits on planetary inclination. Most importantly, we integrate for a long time, secular in nature.

2 METHODS

2.1 Previous work

HW99 provide an extensive computational study on the stability limits of circular planetary orbits in general binary systems, producing an empirical fit for $a_{\rm crit}$, the semi-major axis of the innermost stable (initially circular) planetary orbit. The compute $a_{\rm crit}$ after integrating the planetary orbits (via direct N-body calculations) across a range of binary eccentricities $e_{\rm b}$ and binary mass ratios $\mu_{\rm b}=M_2/(M_1+M_2)$, producing a parametric fit of $a_{\rm crit}$ as a function of $e_{\rm b}$ and $\mu_{\rm b}$ greatly expanding on the original study of this problem by Dvorak (1986). There have been exploratory computational works on inclined circumbinary orbits. Pilat-Lohinger et al. (2003) explored stability around binaries with equal mass and planets with inclinations up to 50°, while Doolin & Blundell (2011) explored the effect of planetary inclination on stability across a wide range of binary configurations, without addressing the dependence of $a_{\rm crit}$ on planetary inclination.

2.2 Setup

2.2.1 *Initial orbits*

We probe the stability of planets as a function of initial barycentric radius r_0 by direct numerical integration of the binary and planetary orbits (this is a similar setup to that of Dvorak & Froeschle 1989 and HW99). We work in units where $a_{\rm b}=M_{\rm b}=M_1+M_2=1$ where $a_{\rm b}$ is the binary semi-major axis and $M_{\rm b}$ is the total binary mass. We vary both the mass ratio of the binary $\mu_{\rm b}=M_2/M_{\rm b}$ and its eccentricity $e_{\rm b}$. The binary is fixed to live in the x-y plane (with the binary's angular momentum pointing in the z-direction) and it is initialized at pericenter for half of our integrations and at apocenter for the other half. Planets are massless test particles. Their positions are evenly spaced in radius (spacing is $\Delta r=0.033a_{\rm b}$) and evenly spaced in azimuth (8 angular positions per value of a). We initialize and integrate a grid of planets for every combination of 9 values of $\mu_{\rm b}\in[0.1,0.5]$, 15 values of $e_{\rm b}\in[0,0.7]$ and 10 values of $i\in[0^\circ,90^\circ]$ using uniform sampling intervals. For each numerical integration, all planets share the same initial inclination i respect to the binary. In addition to the introduction of planetary inclinations, our work differs form preceding ones in the extended duration of the integrations (see Section below).

The planet velocities are initialized in the azimuthal direction and are given a magnitude of $v_{\phi,0}=\sqrt{\mathcal{G}M_{\rm b}/r_0}$. This configuration is equivalent to setting zero-eccentricity Jacobian orbital elements[1]. This velocity is slightly smaller than the circular velocity required for a quasi-Keplerian potential with a quadrupole term:

$$v^2_{\rm circ}(r)\simeq\frac{\mathcal{G}M_{\rm b}}{r}\left[1+\frac{3}{4}\mu_{\rm b}(1-\mu_{\rm b})\left(\frac{a_{\rm b}}{r}\right)^2\left(1+\frac{3}{2}e^2_{\rm b}\right)\right]\ , \tag{1}$$

which implies that planets initialized with velocity $v_{\phi,0}$ are in sub-centrifugal equilibrium, and therefore ay the apocenter phase in a slightly eccentric orbit of semi-major axis $\tilde{a}_0$, i.e., $r_0\approx\tilde{a}_0(1+\tilde{e}_0)$ and $v^2_{\phi,0}\simeq v^2_{\rm circ}(1-2\tilde{e}_0)$, where the "artificial eccentricity" (Rafikov 2013; Paardekooper et al. 2012) is

$$\tilde{e}_0(r)=(3/4)\mu_{\rm b}(1-\mu_{\rm b})\,(a_{\rm b}/r)^2\left(1+\tfrac{3}{2}e^2_{\rm b}\right)\ . \tag{2}$$

If one numerically integrates the orbit of particles started with with $v_{\phi,0}$ under a binary potential, the resulting orbits exhibit *on average* radial oscillations of epicyclic amplitude $\sim\tilde{a}_0\tilde{e}_0$, but fast (forced) oscillations on timescales of order $T_{\rm b}$ are still present (see Section 2.2.2 below).

2.2.2 *Expected behavior*

A brief discussion of secular and dynamical time-scales informs our expectations from the N-body integrations (e.g., Doolin & Blundell 2011). As our integration time is significantly longer than in previous works, we expect to capture some of the long-term effects predicted by secular theory. In particular, secular time-scales will be used to justify our choice of the line of nodes Ω=0 for all our integrations, and short time-scales will be used to inform our choice of radial spacing Δr.

2.2.2.1 Long secular time-scales: Over long secular time-scales (ignoring dynamical instabilities), the orbital dynamics – represented by the planets angular momentum and eccentricity vectors – can be described by the double-averaged potential per unit mass truncated to quadrupole order (e.g. Farago & Laskar 2010; Liu et al. 2015)

$$\Phi_2=\frac{1}{8}\frac{\mathcal{G}\mu_{\rm b}a^2_{\rm b}}{a^3(1-e^2)^{3/2}}\left[1-6e^2_{\rm b}-3(1-e^2_{\rm b})(\hat{\mathbf{z}}\cdot\hat{\mathbf{n}})^2+15e^2_{\rm b}(\hat{\mathbf{x}}\cdot\hat{\mathbf{n}})^2\right]\ , \tag{3}$$

which has been truncated to quadrupole order in the semi-major axes and where $\hat{\mathbf{n}}$ is the direction of the planets angular momentum, and $\hat{\mathbf{x}}$ and $\hat{\mathbf{z}}$ define a coordinate system aligned with the central binary ($\hat{\mathbf{x}}$ parallel to the binary's eccentricity vector and $\hat{\mathbf{z}}$

[1] i.e., initial semi-major axis is $a=r$, defined in a frame where planets orbit a single object of mass $M_{\rm b}$ located at barycenter of the binary.

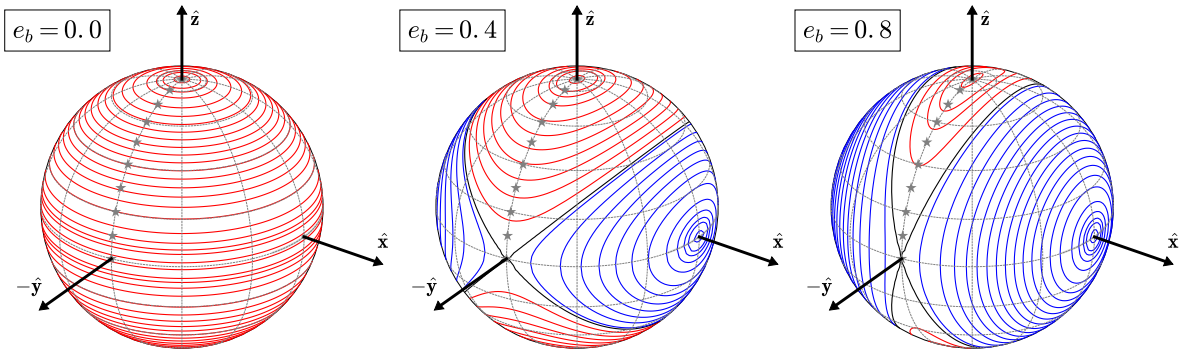

Figure 1. Constant energy levels on the unit angular momentum sphere for circular orbits (from Eq. 3 evaluated with $e = 0$ for all orientations of $\hat{\mathbf{n}}$). For circular binaries ($e_\mathrm{b} = 0$, left panel) the motion of the unit angular momentum vector $\hat{\mathbf{n}}$ is restricted to precession around $\hat{\mathbf{z}}$, the angular momentum vector of the central binary, while the mutual inclination i (where $\cos i = \hat{\mathbf{n}} \cdot \hat{\mathbf{z}}$) remains constant. At finite eccentricity ($e_\mathrm{b} = 0.4$, middle panel), $\cos i$ is not strictly constant, and thus the $\hat{\mathbf{n}}$ vector experiences nutation in addition to precession. For $e_\mathrm{b} \neq 0$, there are two additional fixed points around which precession is possible: $\hat{\mathbf{n}} = \hat{\mathbf{x}}$ and $\hat{\mathbf{n}} = -\hat{\mathbf{x}}$. Thus the unit sphere is divided into two distinct precession regions (red and blue, depicting precession arounf $\hat{\mathbf{z}}$ and $\hat{\mathbf{x}}$ respectively) delimited by a separatrix (in black). For high eccentricity ($e_\mathrm{b} = 0.8$, right panel) most of the unit sphere is dominated by precession around $\hat{\mathbf{x}}$, except for a narrow region which includes the case of binary-planet coplanarity. Star symbols depict the different *initial* inclinations explored in this study (0° to 90°in intervals of 10°); all for $\Omega = 0$, i.e., at least initially, all the orbits explored in this work are contained in the red region of the angular momentum unit sphere.

parallel to its angular momentum vector). In Eq. (3), Φ_2 depends only on the magnitude of the eccentricity vector $|\mathbf{e}|{=}e$, which as a result, is conserved: i.e., *circular orbits remain circular* at the quadrupole-level of approximation. Our choice of initial $\Omega{=}0$ *for all* planetary orbits implies that all planetary vectors lie on one and the same plane in the coordinate system defined by the binary. For $e_\mathrm{b}{=}0$, Φ_2 exhibits two equilibrium points ($\hat{\mathbf{n}}$ is aligned or anti-aligned with $\hat{\mathbf{z}}$), implying that any initial $\hat{\mathbf{n}}$ will trivially precess around $\hat{\mathbf{z}}$ at a rate given by $d\hat{\mathbf{n}}/dt \propto (\hat{\mathbf{n}} \cdot \hat{\mathbf{z}})(\hat{\mathbf{n}} \times \hat{\mathbf{z}})$, i.e., the mutual inclination between planet and binary is conserved. However, when $e_\mathrm{b}{\neq}0$, the constant-energy levels in Φ_2 exhibit two additional (stable) fixed points, implying that $\hat{\mathbf{n}}$ can precess either around $\hat{\mathbf{z}}$ or around $\hat{\mathbf{x}}$, and that, in general, the mutual inclination will not be constant (Farago & Laskar 2010; Doolin & Blundell 2011). In Fig. 1, we show the equi-potential contours of Φ_2 in the unit sphere of possible orientations of $\hat{\mathbf{n}}$ (assuming $e{=}0$). Our initial conditions imply that the planet angular momentum vector $\hat{\mathbf{n}}{=}(\sin i \sin\Omega, -\sin i \cos\Omega, \cos i)$ initial lies in the $\hat{\mathbf{y}}{-}\hat{\mathbf{z}}$ plane, therefore always living in the region that precesses around $\hat{\mathbf{z}}$ (in red). This is in contrast with the study by Doolin & Blundell (2011) in which $\hat{\mathbf{n}}$ is initialized with $\Omega{=}90^\circ$, i.e., in the $\hat{\mathbf{x}}{-}\hat{\mathbf{z}}$ plane, which includes both regimes of precession around $\hat{\mathbf{z}}$ (in red) and $\hat{\mathbf{x}}$ (in blue). Deviations from the secular behavior are expected close to the binary – especially for those inclinations close to the separatrix in Fig. 1 – both owing to mean-motion resonances as to higher order terms in the potential (e.g., octupole terms).

2.2.2.2 Short dynamical time-scales: On time-scales of order the planet orbital period, the fast oscillations (averaged out by the secular approximation) imprint an initial, *phase-dependent*, perturbation to the planetary orbits (Fig. 2). Short-term variability introduces an intrinsic "fuzziness" into the very definitions of semi-major axis a and eccentricity e. Oscillation amplitudes can be described by free and forced eccentricities (acting on timescales $\Omega_K^{-1}{=}\sqrt{r/(\mathcal{G}M_\mathrm{b})}$ and $\Omega_\mathrm{b}^{-1}{=}\sqrt{a_\mathrm{b}/(\mathcal{G}M_\mathrm{b})}$; see equations 27 and 39 in Leung & Lee 2013) and only on average does the free eccentricity coincide with $\tilde{e}_0$ from Eq. 2 (see Fig. 2). In practice, each particle initialized with azimuthal velocity $v_{\phi,0}$ and angular phase ϕ_0 will possess a unique free eccentricity $e_\mathrm{free} = \tilde{e}_0 + \delta\tilde{e}(\phi_0, e_\mathrm{b}, \mu_\mathrm{b})$, and a guiding center semi-major axis of $\tilde{a} = \tilde{a}_0 + \delta\tilde{a}(\phi_0; e_\mathrm{b}, \mu_\mathrm{b})$, such that $\tilde{a}(1 + e_\mathrm{free}) \approx r_0$ for all ϕ_0. At closest approach, $r = \tilde{a}(1 - e_\mathrm{free}) \approx r_0(1 - 2\tilde{e}_0) + 2\delta\tilde{a}$, which defines an intrinsic fuzziness in semi-major axis for all particles with equal Jacobian semimajor axis $a = r_0$ but with different initial phases (see the spread in the blue curves in Fig. 2). For $e_\mathrm{b} = 0$ and $\mu_\mathrm{b} = 0.5$ we have measured this spread to be $\delta\tilde{a} \approx 0.01a_\mathrm{b}$ at $r = 3a_\mathrm{b}$. This quantity informs our choice of a fiducial radial spacing to be $\Delta r = 0.033a_\mathrm{b}$ throughout this work unless stated otherwise. Note that orbits around binaries with an equal mass ratio and high eccentricity may exhibit spreads of up to $\delta\tilde{a} \approx 0.2a_b$. When identifying stability boundaries this uncertainty $\delta\tilde{a}$ might become an issue as the initial conditions are usually grouped by Jacobian semi-major axis $a = r_0$ and not by $\tilde{a}$; consequently, the spread in closest approach might consistently induce ejections for some values of ϕ_0 but not for others (we do indeed see this effect; Section 3.1). We have found that $\langle a \rangle$, the median (Jacobian) a ($\approx \tilde{a}$) computed over an initial integration time (a couple hundred binary orbits), is often a convenient radial coordinate, and a useful label, for the initial orbits. Whenever $\langle a \rangle$ is used in our analysis instead of a, this will be made explicit in the text.

2.3 Numerical technique

We use the Bulirsch-Stoer (BS) integrator (e.g., Press et al. 1986) in the MERCURY package (Chambers 1999) to carry out our integrations. The accuracy parameter in the BS scheme set to 10^{-13}. We work in units where $a_\mathrm{b} = 1$. The total integration time is $T_\mathrm{int} = 3 \times 10^5 T_\mathrm{b}$ where $T_\mathrm{b} = 2\pi\sqrt{a_\mathrm{b}/\mathcal{G}M_\mathrm{b}}$ is the period of the binary with the initial timestep is $10^{-2}T_\mathrm{b}$. This integration time is the fiducial value unless stated otherwise. In some specific situations, we have extended T_int to $4 \times 10^5 T_\mathrm{b}$ if some ejections far from the binary are still taking place close to the end of the original integration. In most of these cases, the extra integration time did not change our results. We choose the ejection distance to be at $25a_\mathrm{b}$. This is between 5 to 15 times the stability limits across the vast majority of our different orbital configurations. For simplicity,

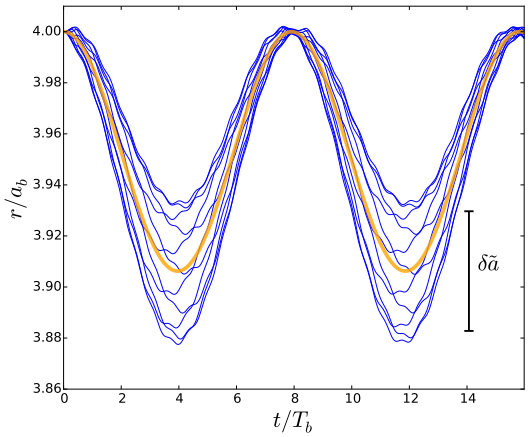

Figure 2. Short term evolution of the barycentric radius $r/a_{\rm b}$ of 10 CBPs (blue lines), emphasizing the difference between Jacobian zero eccentricity and geometrically circular orbits (Pichardo et al. 2005; Youdin et al. 2012). Planet orbits are evolved around a circular, equal-mass binary where all planets are initialized at the same barycentric radius ($r_0 = 4a_{\rm b}$) and orbital velocity ($v_\phi = \sqrt{\mathcal{G}M_{\rm b}/r_0}$), but with initial azimuthal orientation ϕ_0 spanning the range $[0, \pi]$. The thick orange line (which closely resembles an average of all individual trajectories) corresponds to the evolution of the same initial conditions, this time around under a potential that has been expanded to second order in $r/a_{\rm b}$ and time-averaged once over the period of the binary. In this case, the axisymmetry imposed implies that all orbits overlap, and the resulting trajectory is very closely described by a Keplerian orbit of eccentricity $\tilde{e}_0 \approx 0.014$ and semi-major axis $\tilde{a}_0 = r_0/(1+\tilde{e}_0) \approx 3.945a_{\rm b}$ (see text). averaged potential. The spread in barycentric radius at pericenter is well described by the quantity $\delta\tilde{a}$ discussed in the text.

we do not consider direct collisions onto the stars. The distinction between ejections and collisions in this case may be superfluous, as particles with eccentricities high enough to collide with one of the stars are in most cases already in trajectories leading to ejections. This is consistent with the analytic arguments of Smullen et al. (2016), who explained that test particles near the stability limit typically cannot get too close to either star while still conserving the Jacobi constant. Their numerical results, as well as those from Sutherland & Fabrycky (2016), support this claim, as they find collisions are infrequent.

2.4 Analysis

We define a "long-term stable" barycentric radius r as that in which all (16) coorbital planets survive the entire length of the integration. The distance $a_{\rm crit}$ is the *closest* distance to the binary that is long term stable. HW99 and Dvorak (1986) originally studied this problem in a similar way, the latter referring to $a_{\rm crit}$ as the Lower Critical Orbit (LCO). Dvorak (1986) also introduced the Upper Critical Orbit (UCO), the *furthest* orbital distance at which there are still ejections at the end of the integration. In this work, we refer to this quantity as $a_{\rm st}$, which also corresponds to the orbital distance outside of which orbital stability is met for all values of r_0, i.e., at $a_{\rm st}$ and beyond, all planets in our grid survive the integrations. Note that $a_{\rm st}$ is almost always located just outside the $n:1$ MMR where the outermost ejection occurs.

Table 1. Stability Regions for Typical Configuration

Region	Location or Width [$a_{\rm b}$]
(0) Unstable Inner Region	$\leqslant\sim 2.0-4.2$
(1S) 1st Island of Stability (ends at $a_{\rm crit}$)	0.07 ± 0.03
(1U) 1st Island of Instability at $n:1$ MMR	0.10 ± 0.03
(2S) 2nd Island of Stability	0.36 ± 0.10
(2U) 2nd Island of Instability at next $n:1$ res.	0.03 ± 0.03
(3) Stable Outer Region (starts at $a_{\rm st}$)	$\geqslant a_{\rm crit} + (0.3 \pm 0.3)$

3 RESULTS

3.1 Patterns of Stability

The long-term planetary dynamics exhibit a nearly ubiquitous pattern of stability, in which three qualitatively different regions can be identified as a function of median semi-major axis a (Table 1). We describe these three stability regions below.

Region 0 – Unconditional instability: Nearly all of the orbits in the innermost region (within $a \lesssim a_{\rm crit}$) eject on timescales shorter than $10^3 T_{\rm b}$. For $a < a_{\rm crit}$, we find that the ejection time follows the relation $\log T_{\rm ejec} \propto a$, and it rises steeply when a approaches $a_{\rm crit}$. Figure 3 shows the ejection time $T_{\rm ejec}$ as a function of planet semi-major axis around a binary of $\mu_{\rm b}$=0.2 and $e_{\rm b}$=0.2 for i=0° (left panel) and i=20° (right panel). Long-term stable orbits are depicted by blue circles, nominally placed at $T_{\rm ejec}$=$T_{\rm int}$. In both cases ($i = 0°, 90°$), $a_{\rm crit} \sim 3a_{\rm b}$ roughly defines a boundary between long-term stable orbits and orbits for which $T_{\rm ejec} \sim 10^2$-$10^3 T_{\rm b}$. Interestingly, some long-term stable orbits can be found for $a < a_{\rm crit}$, but the stability requirement fails to pass for one of the two binary binary configurations considered (either binary phase at apocenter or at pericenter at t=0). This can be explained by the intrinsic fuzziness in the definition of all a close to the binary (Sections 2.2.1 and 2.2.2). As discussed in Sec 2.2.2.2 the dependence of the short-term orbital evolution on the initial phase of the orbit can introduce patterns in which, for the same r_0, only certain initial mean anomalies result in ejection while others turn out the be long-term stable. In agreement with the fitting formula of HW99, these partially stable orbits are excluded by critical boundary represented by $a_{\rm crit}$.

Regions 1S, 1U, 2S, 2U - Conditional stability: In the region where $a_{\rm crit} \lesssim a \lesssim a_{\rm st}$, most numerical experiments exhibit a shared pattern, which consists (from small to large a) of: one wide stability strip or "island" (1S) followed by an unstable one (1U), further accompanied by another stable region (2S) and by one final, narrow unstable strip (2U). This general pattern emerges in about 75% of our numerical experiments. The 1S and 1U islands are typically of the same width in a. These regions can be seen in the examples of Fig. 3. The 1U region is often located near the first $n:1$ MMR outside 1S. Meanwhile, the 2U region is located near the first $n:1$ MMR available after 2S. The 2U island is significantly narrower than 1S. It thus becomes apparent that subsequent instability islands (3U, 4S,...; e.g., see HW99; Kostov et al. 2013) are not picked up because of the coarse initial radial spacing Δr (see below).

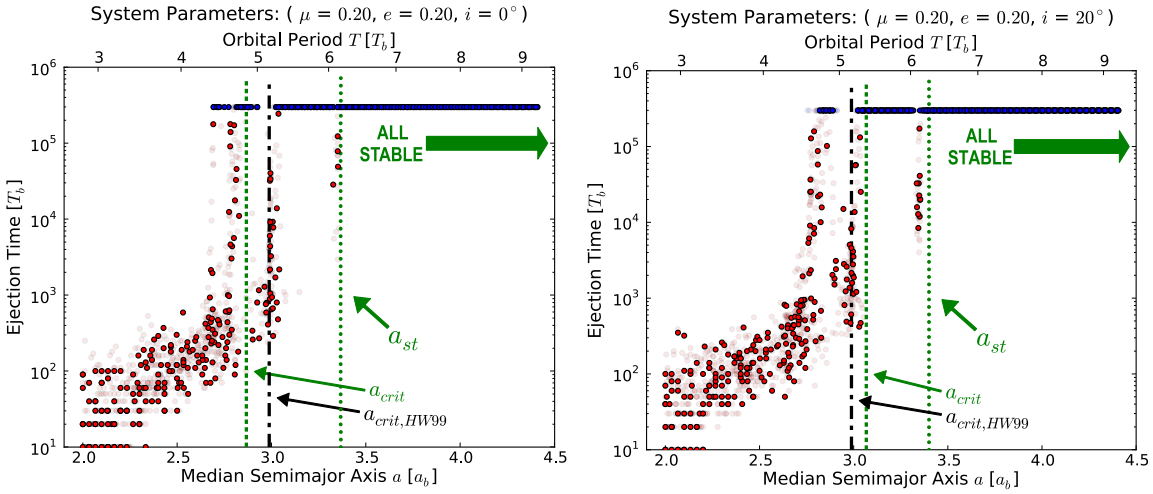

Figure 3. Both: Binary $\mu_{\rm b} = 0.2$, $e = 0.2$. Top: $i = 0°$. Bottom: $i = 20°$. The distribution of surviving planets (blue) and ejection times of unstable planets (red) illustrate the different regions of stability along with the corresponding values of $a_{\rm crit}$ and $a_{\rm st}$ in this typical case. Additionally, the faded points show what would be added with a resolution 3 times finer in $a_{\rm p}$. For these configurations – as with most cases – not much is added. Vertical lines mark off $a_{\rm st}$ – which hardly changes in the inclined case, and $a_{\rm crit}$ – which moves from the 1$^{\rm st}$ island of stability just inside the 5 : 1 MMR in the $i = 0°$ case to the 2$^{\rm nd}$ just outside in the $i = 20°$. The value of $a_{\rm crit}$ from the fitting formula of HW99 is also marked off as a dashed vertical line and shows agreement with our values for both cases. Overall, this coplanar case and the corresponding case at $i = 20°$ are mostly the same. One difference is that the 2$^{\rm nd}$ island of instability in the inclined case is slightly stronger than that in the coplanar case.

Region 3 - Unconditional stability: In most cases, beyond the second strip of instability, all orbits in our integrations are stable. This defines the semi-major axis $a_{\rm st}$ (Section 2.4). In less than 5% of configurations, an additional (third) strip of instability appears (Fig. 4 shows one such case). No configurations in our parameter space had a fourth strip of instability. Since each successive unstable strip has a thinner width and longer ejection time than the previous one, it is possible that longer integration times, and finer sampling in a would reveal this vanishingly small unstable regions. These findings apply to our fiducial radial spacing of Δr=0.033$a_{\rm b}$. We have experimented with different values of Δr (down to Δr=0.01$a_{\rm b}$; see Section 3.2 below), no fourth island of instability was found for finer samplings.

3.2 Robustness and convergence

The values obtained for $a_{\rm crit}$ and $a_{\rm st}$ can potentially depend on our total integration time and their precision may also depend on the choice of radial spacing. In this section, we explore the robustness of our results when varying our fiducial values of $t_{\rm int}$ and Δr.

3.2.1 Convergence of $a_{\rm crit}$ with integration time

X We extended the integrations in the vicinity of $a_{\rm crit}$ by a factor of 1000 to 3 $\times$ 10$^8 T_{\rm b}$ across our parameter space for two different inclinations: $i = 0°$ and $i = 30°$. In these two cases, we found no significant difference in the resulting values of $a_{\rm crit}$. In particular, for $i = 0°$, we largely reproduce the HW99 results for $a_{\rm crit}$, including their parametric fit of $a_{\rm crit}$ as a function of $e_{\rm b}$ and $\mu_{\rm b}$. we have confirmed that the integration time used by HW99 of 10^4 $T_{\rm b}$ is sufficient to yield the same value of $a_{\rm crit}$ in 90% of the cases to within $\pm 0.1 a_{\rm b}$.

The fiducial spacing of Δr=0.033$a_{\rm b}$ suffices for identifying the innermost region of stability and to detect narrow instability islands/patches outside this central region as well as the widths of the innermost islands of instability. Beyond this fiducial Δr (experimenting with higher resolutions down to 0.005$a_{\rm b}$), we have found no significant differences, thus the value of $a_{\rm crit}$ can only improve in precision, yet not in accuracy. On the other hand, lower resolutions do have trouble in pinpointing $a_{\rm crit}$, and furthermore, they can miss altogether some of the inner islands of stability.

As a final convergence test, we explored the finer structure around $a_{\rm crit}$ over a very long time. We extended a subset of our configurations to integration times of $t_{\rm int} = 10^9$ $T_{\rm b}$ (now approaching a fraction of the physical age of a *close* stellar binary). for rings of test particles with $r_0 = a_{\rm crit}$ (as determined by the runs with fiducial integration times). The binary parameters $\mu_{\rm b}$ and $e_{\rm b}$ are both sampled in intervals of 0.1, and the binary initial phase is set to periapse only. We evaluate i at two angles: 0° and 30° (40 configurations for each). We find that the long-term stability at $a_{\rm crit}$ persists over timescales much longer than our fiducial experiments. Some isolated ejection are still possible. In the coplanar configurations, for example, 20 out of 40 result in at least one ejection. Of these, 90% had an ejection before $4 \times 10^7 T_{\rm b}$. In the inclined configurations, 22 out of 40 result in at least one ejection. Of these 90% had an ejection before $5.5 \times 10^7 T_{\rm b}$. Of all the configurations with at least one ejection (42 out of 80), only 10 have more that half of the planets (out of 8 possible) eject. These results give further reassurance that $a_{\rm crit}$ – for inclined and coplanar orbits – is a good reference distance for the innermost stable circumbinary orbit for a significant fraction of the lifetimes of these systems.

3.2.2 Convergence of $a_{\rm st}$ with radial spacing

In contrast with $a_{\rm crit}$, $a_{\rm st}$ can depend critically on both $t_{\rm int}$ and Δr. A time-converged determination of $a_{\rm st}$ can be assessed by taking our long integrations and replicating our computation $a_{\rm st}$ at intervals $[0, t]$ for different $t < t_{\rm int}$. We define the "required integration time" as the shortest t for which $a_{\rm st}$ is indistinguishable from the value of $a_{\rm st}$ obtained from the full length integration $[0, t_{\rm int}]$.

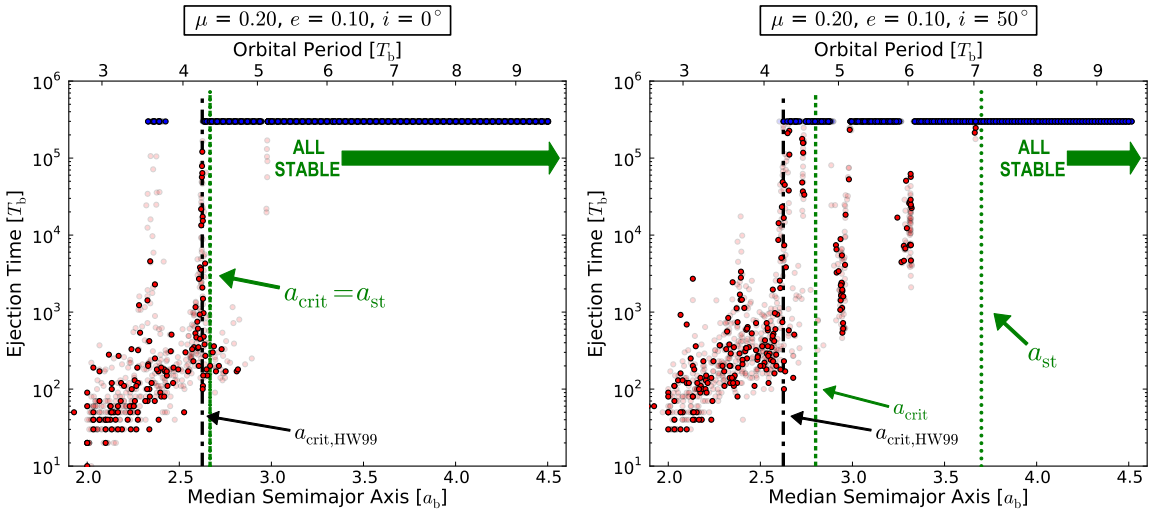

Figure 4. Both: Binary $\mu_b = 0.2$, $e = 0.1$. Top: $i = 0°$. Bottom: $i = 50°$. See Figure 3 for a description of the plot. In this extreme case, there is a significant difference between the coplanar case and the corresponding case with $i = 50°$. Whereas the coplanar case has no islands of instability with normal resolution, the inclined case has three such islands. This results in a wide gap between a_{crit} and a_{st}. For the coplanar case, finer resolution reveals a very thin island at the 5 : 1 MMR. Though, since it does not appear with higher resolution, we do not consider it significant. Another unusual aspect of the inclined case is a trace of an island of instability at the 9 : 2 MMR. We did not explore this feature. Usually, the differences between coplanar orbits and inclined orbits around a particular binary configuration fall between the lack of differences in Figure 3 and the drastic differences in this figure. For a typical case, a_{crit} from the coplanar case eventually overtakes the 1^{st} island of stability at a sufficient inclination ($\sim 30 - 40°$), while a new 2^{nd} island of instability arises at the next n : 1 MMR.

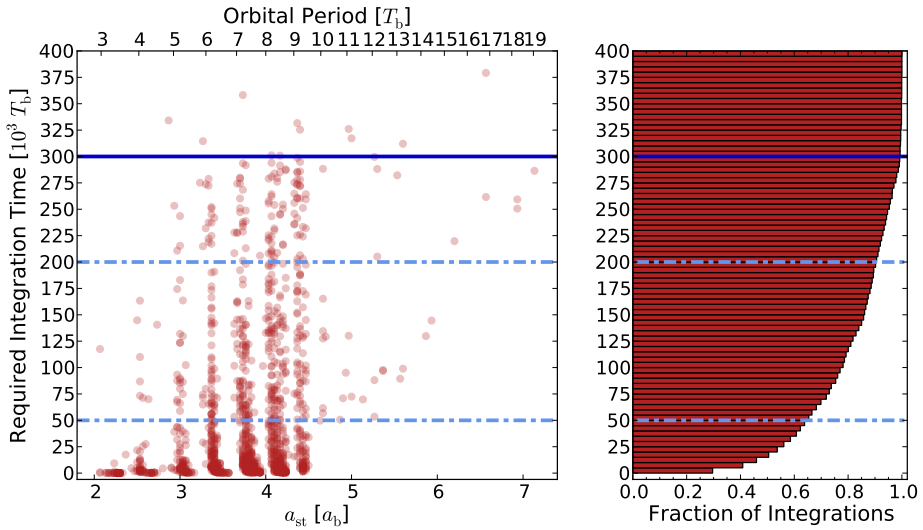

Figure 5. Distribution of required integration times for each value of a_{st} across the 1350 configurations in our entire parameter space. We define the required integration time to be the minimum time need to identify the same value of a_{st} that the longer integrations of $3 \times 10^5 T_b$ (the solid line) find to within $0.1 a_b$. For 69% of the simulations, $50,000$ T_b (the lower dashed line) would be sufficient to identify the same a_{st}. For 91% of the simulations, $200,000$ T_b (the upper dashed line) would be sufficient. Configurations with smaller values of a_{st} and smaller inclinations have lower required integration times on average.

Fig. 5 depicts the required integration time for each determined value of a_{st} corresponding to each of the different configurations tested in this work (1350 binary and inclination configurations). For the smallest values of a_{st} (typically for small e_b), the required integration time is about $15,000$ T_b, meaning that a few times 10^4 binary orbits (as in HW99) would be sufficient to find a well-defined value of a_{st}. However for about 50% of the configurations (especially for those that result in $a_{st} \gtrsim 3a_b$) the required integration time can extend up to $300,000$ T_b. The required integration time begins to converge as it approaches the integration time that we used across the majority of our parameter study. Running the integrations for the final $100,000$ T_b only changes a_{st} for about 10% of our configurations.

We experimented with longer timescales of 5×10^5 T_b for those configurations that were still resulting in a large number of ejections toward the end of the integration (i.e., ongoing ejections at the last measurable island of instability at $t \sim t_{eq}$). In high inclination configurations ($i \gtrsim 70°$), the extra integration time produces an additional island of instability and thus, increases a_{st} in about

one-third of all such cases. For low inclinations, the extra integration time very rarely changes $a_{\rm st}$.

Longer integrations may result in additional ejections at greater distances than the determined value of $a_{\rm st}$. This introduces ambiguity to the identification of $a_{\rm st}$ with the boundary that gives way to "unconditionally stable orbits". If these ejections are "isolated" (i.e., one or two planets ejected for one value of r_0 and no neighboring ejections) such that it is impossible to identify an unstable strip with unambiguous width, then the value of $a_{\rm st}$ in unchanged. As seen in Fig. 5, only a very small fraction of configurations suffer ejections after $3 \times 10^5 T_{\rm b}$. Similarly, only a small fraction of systems exhibit ejections at distances greater than $\sim 4.5 a_{\rm b}$, showing that, at least statistically, $a_{\rm st}$ can be properly determined for the value of Δr chosen.

The value of $a_{\rm st}$ can exhibit some dependence on Δr. In fact, a finer radial sampling can uncover narrow, high-order MMRs that eject planets only after a very long time. Since the successive islands of instability have thinner widths, the fiducial spacing of $\Delta r = 0.033 a_{\rm b}$ might be overlooking them altogether. We chose several configurations representing a variety of different parameters across our entire parameter space and integrated them out to either 2×10^7 $T_{\rm b}$ or 2×10^8 $T_{\rm b}$ with a 3 times higher resolution in semi-major axis of $\Delta r = 0.011$. We find that the characteristic structure of stability from our shorter integrations remains over these longer timescales. The widths of the unstable islands and the extent of the inner unstable region increase slightly, but not by an appreciable amount. In general, the structure of stability from integrations on the order of one hundred thousand binary orbits is a valid representation of the orbital stability around a stability over its lifetime.

In order to further isolate the effect of finer radial sampling, we ran a few long-term integrations of ($t_{\rm int} = 10^9 T_{\rm b}$) with radial coordinates r_0 in the vicinity of the innermost n : 1 MMR that was stable in our fiducial integrations (spanning a width of $0.02 a_{\rm b}$ with a spacing of $\Delta r = 0.005 a_{\rm b}$). For each value of r_0, we used the same parameter space of 80 configurations in $\mu_{\rm b}$, $e_{\rm b}$, and i and initialize planets only ϕ_0=0° and ϕ_0=180°. As expected, we find additional ejections beyond $a_{\rm st}$ (as determined by the runs with fiducial spacing), although none of the $\phi_0 = 180°$ cases eject. In several configurations, these additional ejections are rare. For example, only 3 of the 40 *coplanar* integrations result in additional ejections. In contrast, *inclined* configurations exhibit additional distant ejections in 11 out of 40 cases. These new island beyond the nominal $a_{\rm st}$ have widths of about $0.01 a_{\rm b}$ on average (i.e., partially unresolved by our spacing of $0.005 a_{\rm b}$). For binaries with semi-major axis of ~ 0.2 AU (e.g.,Kepler-16; Doyle et al. 2011), this instability region would have a width of $\lesssim 0.002$ AU or 12 Neptune radii. Repeating the analysis leading to Fig. 5, we find that the minimum ejection times of these islands are almost always above 10^6 $T_{\rm b}$, with very few ejections occur above 10^8 $T_{\rm b}$.

3.3 Outlier outcomes

A subset of binary configurations have a small range of high inclination orbits that cannot be classified according to the stability pattern described in Section 3.1. At each inclination of $i \geqslant 50°$, there is a narrow range of binary eccentricities ($\Delta e \leqslant 0.05$) that have uncharacteristically large values of $a_{\rm st}$ for unequal-mass binaries. For the vast majority of configurations, the maximum value of $a_{\rm st}$ is $\lesssim 4.5$ (in the vicinity of an orbital period of $9 T_{\rm b}$). Meanwhile, the "peculiar" configurations yield values of $a_{\rm st}$ that correspond to

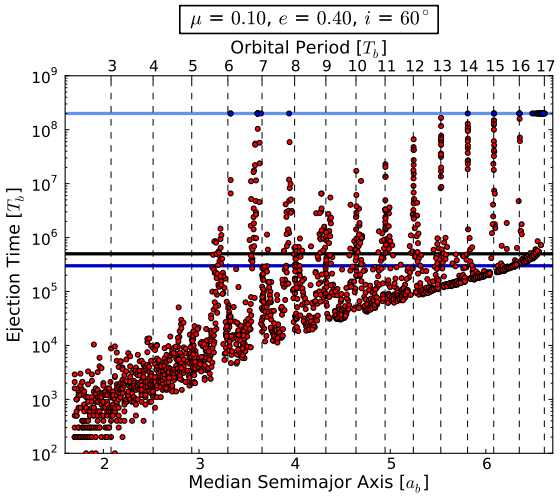

Figure 6. The configurations with $\mu_{\rm b} \leqslant 0.4$, $e = 0.4$, and $i = 60°$ have much larger values of a_{st} than those across the rest of our parameter space. For $\mu_{\rm b} = 0.1$, a standard integration time of $3 \times 10^5 T_{\rm b}$ (lower blue line) reveals thin islands of stability with widths of 0.07 ± 0.03 near each $n : 1$ MMR from n = 6 to n = 16. These islands are embedded in an otherwise completely unstable region out to $a_{\rm st}$ = 6.6. Extending the integration to $2 \times 10^8 T_{\rm b}$ (upper light blue line) shows that the middle islands of stability between n = 9 and n = 13 all eject. It is unclear whether the inner and outer islands would survive if we further extended the integration. The stable orbits at $n : 1$ MMRs with $n \geqslant 9$ are more sharply concentrated at the MMRs compared to those at the lower order islands. Lastly, an integration time of $5 \times 10^5 T_{\rm b}$ (middle black line) is needed to identify $a_{\rm st}$. For this particular case where $\mu_{\rm b} = 0.1$, $e_{\rm b} = 0.4$, and $i = 60°$, only the innermost and outermost islands of stability survive the longer integration

orbital periods between 10-20 $T_{\rm b}$, in addition to exhibiting distinct stability patterns for regions inside $a_{\rm st}$.

The measured value of $a_{\rm crit}$ does not change in these outlier configurations, which exhibit the first stability island (1S in Section 3.1) in all cases. However, $a_{\rm st}$ can be dramatically changed; whereas typical configurations have at least one additional wide region of stability between $a_{\rm crit}$ and $a_{\rm st}$,the outlier configurations may have their innermost unstable region 1U extend all of the way out to $a_{\rm st}$. Furthermore, when the additional stability islands (2S and beyond) do appear, they are narrower than in the typical cases, and when integrating for longer times, they also start disappearing as ejections continue to take place in the long run. Figure 6 shows an example of this unusual pattern of stability over an integration time of 2×10^8 $T_{\rm b}$.

These unusual measurements of $a_{\rm st}$ appear as local spikes in an otherwise smooth and monotonic curve of $a_{\rm st}$ as a function of $e_{\rm b}$. In the absence of these additional peaks, the curve of $a_{\rm st}$ as a function of $e_{\rm b}$ is qualitatively similar to that when $i = 0°$. Figure 7 shows that these spikes in $a_{\rm st}$ at particular values of the binary eccentricity $e_{\rm b}$ for three different mass ratios $\mu_{\rm b}$ =0.1, 0.3 and 0.5. Only when $\mu_{\rm b} = 0.5$ (equal-mass binary) the spike is absent. For example, the binary configuration of $\mu_{\rm b} = 0.1$ and $e_{\rm b} = 0.25$ has $a_{\rm st} = 6.9 a_{\rm b}$ when $i = 50°$. If only the mass ratio is changed to $\mu_{\rm b} = 0.5$, then $a_{\rm st} = 3.4 a_{\rm b}$.

From the figure it can be seen that the magnitude and width of this peak appears to grow with decreasing $\mu_{\rm b}$. It is interesting to note that there might be a relation between the appearance of these unusual peaks with the presence a significant octupole term in the gravitational potential. The relative strength of

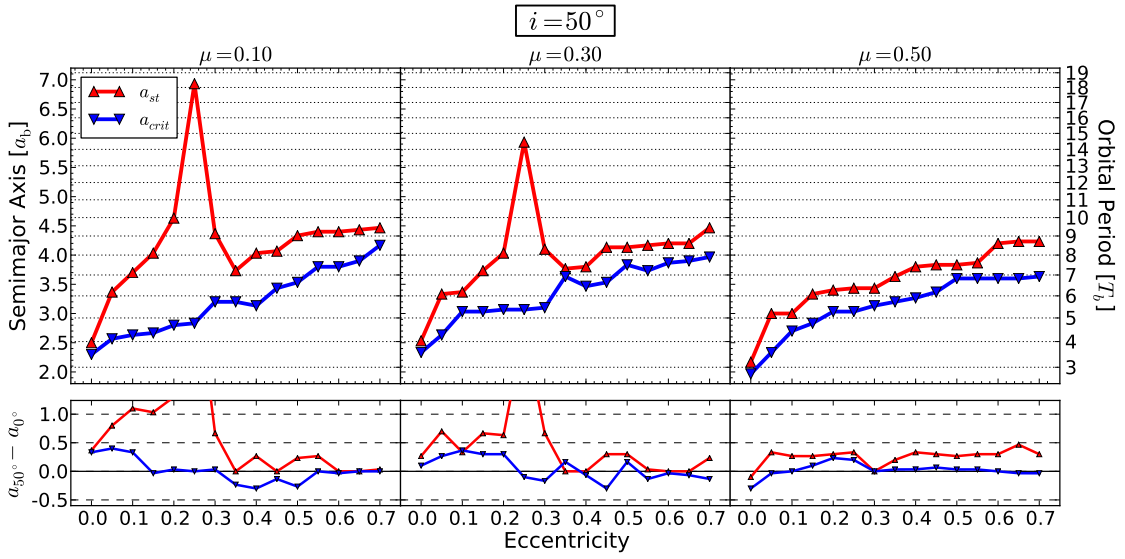

Figure 7. Top: The dependence of $a_{\rm st}$ on binary eccentricity for different binary mass ratios 0.1, 0.3, and 0.5 for planets with inclination of $i = 50^\circ$. Bottom: How the stability limits at $i = 50^\circ$ compare to stability limits for coplanar orbits. There is no strong dependence for how either stability limit changes at high inclination as a function of eccentricity. In some cases, $a_{\rm crit}$ increases. In other cases, $a_{\rm crit}$ decreases. Neglecting the spike at $e = 0.25$, $a_{\rm st}$ increases by a larger amount for low eccentricity binaries. Around high eccentricity binaries, $a_{\rm st}$ increases by a smaller amount, if at all. For $\mu_{\rm b} \leqslant 0.4$, there is a spike in $a_{\rm st}$ that corresponds to one of the outlier configurations described in Section 3.3.

the octupole potential respect to the quadrupole contribution (Eq. 3) scales as $e_{\rm b}(a_{\rm b}/a)\sqrt{1-4\mu_{\rm b}(1-\mu_{\rm b})}$ (see appendix of Petrovich & Muñoz 2016; see also Leung & Lee 2013), and thus vanishes when $\mu_{\rm b} = 0.5$. It is well known that the quadrupole potential of Eq. (3) conserves eccentricity on secular timescales (e.g. Moriwaki & Nakagawa 2004; Farago & Laskar 2010) and that a non-vanishing "forced eccentricity" acting on the circumbinary orbits requires a finite octupole term, as provided by an unequal-mass binary (Moriwaki & Nakagawa 2004). A slowly varying planetary eccentricity due to a significant octupole term might explain some of these features, especially if the islands of stability are observed to gradually degrade over secular timescales. In such case, the secular evolution would trigger the dynamical instability as planetary orbits with $a > a_{\rm crit}$ might reach pericenter values $\approx a_{\rm crit}$ during the high eccentricity phase. This type of "late-onset" dynamical instability aided by secular evolution has been recently explored in the case of hierarchical triple systems by Grishin et al. (2016). In future work, we will explore how octupole-level secular effects can render distant circumbinary planets long-term unstable.

Table 2 summarizes the values of $a_{\rm st}$ for each of the orbital configurations that yield unusual values of $a_{\rm st}$. Binaries with low values of $\mu_{\rm b}$ have the strongest spikes in $a_{\rm st}$. Binaries with $\mu_{\rm b} \approx 0.5$ show little to no increase in the values of $a_{\rm st}$ across the different inclinations explored. The spikes in $a_{\rm st}$ are larger at inclinations of 50° and 60°, and they do not appear for $i \leqslant 40^\circ$. At the current sampling density of i (in intervals of 10°), all these spikes appear for one specific inclination, $a_{\rm st}$ depending very weakly on i otherwise (see Section 3.4 below).

Table 2. $a_{\rm st}$ for Outlier Configurations

i	$e_{\rm b}$	$\mu_{\rm b}$ =	0.1	0.2	0.3	0.4	0.5
50°	0.25		6.93	6.93	5.93	4.90	3.43
60°	0.40		6.60	6.20	5.57	4.87	3.80
70°	0.45		5.60	5.30	4.43	4.10	3.80
80°	0.15		5.27	5.27	5.00	3.73	3.37
90°	0.20		5.30	5.30	4.67	3.73	3.37

These are the configurations that break the usual pattern in $a_{\rm st}$. Each $i \geqslant 50^\circ$ has an eccentricity that results in a set of outlier cases. The values of $a_{\rm st}$ are given at five mass ratios for each combination. The $\mu_{\rm b} = 0.5$ cases are unaffected. For typical cases, $a_{\rm st}$ would be no more than $0.7a_{\rm b}$ larger in the high mass ratio case compared to the equal mass case. These configurations have far larger values of $a_{\rm st}$.

3.4 Fitting formulae for stability boundaries

3.4.1 Dependence of $a_{\rm crit}$ and $a_{\rm st}$ on $e_{\rm b}$ and i

The strongest dependence of both stability limits is on the eccentricity of the binary $e_{\rm b}$, with mutual inclination i playing a secondary role (aside from the exceptional cases described in Section 3.3). Both $a_{\rm crit}$ and $a_{\rm st}$ increase monotonically with $e_{\rm b}$; $a_{\rm crit}$ grows from $\sim 1.9a_{\rm b}$ (when $e_{\rm b} \approx 0$) to $\sim 4.3a_{\rm b}$ (when $e_{\rm b} \gtrsim 0.7$) Similarly, the value of $a_{\rm st}$ is lies between $2a_{\rm b}$ and $4.5a_{\rm b}$. There are general trends as a function of mass ratio as well. For $e_{\rm b}$ fixed, $a_{\rm crit}$ grows with $\mu_{\rm b}$ until peaking at ≈ 0.3 and leveling off for $\mu_{\rm b}$ between 0.3 and 0.5; $a_{\rm crit}$ in turn, is maximum for $\mu_{\rm b} = 0.1$. Additionally, $a_{\rm st}$ grows in a step-function fashion, in consistency with its value being determined by the nearest $n:1$ MMR.

We have found that both $a_{\rm crit}$ and $a_{\rm st}$ depend rather weakly on

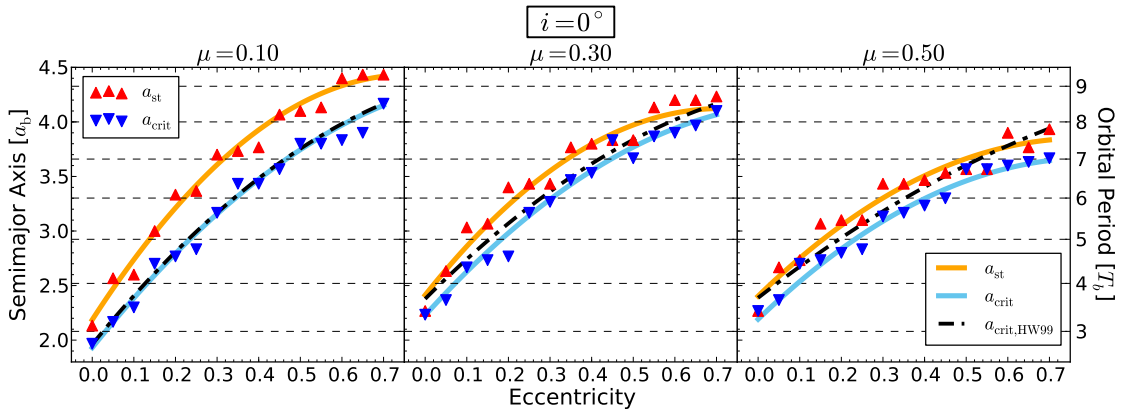

Figure 8. Comparison of our fits for $a_{\rm crit}$, $a_{\rm st}$, and the fitting formula from HW99. Our fit for $a_{\rm crit}$ (lower blue line) agrees very well with their fit (dashed black line) for $\mu_{\rm b} \leqslant 30^\circ$. However, our fit yields about 10% lower values of $a_{\rm crit}$ for equal mass binaries with high eccentricity. The fit for $a_{\rm crit}$ matches the data points well (upside-down triangles) for all mass ratios. Since the values of $a_{\rm st}$ are typically just above $n:1$ MMRs, the fit for $a_{\rm st}$ is not able to reproduce the step-function nature of the data points (right-side-up triangles) as well with a second-order polynomial. However, "rounding" the fit to the nearest $n:1$ MMR offsets this issue in most cases. H99 used lower resolution which explain the small discrepancies

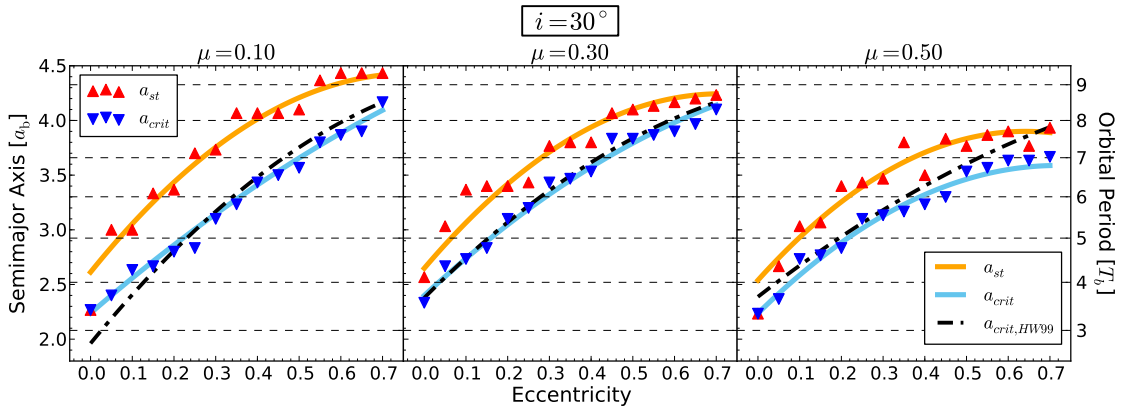

Figure 9. See Figure 8 for a description of the plot. At a low inclination of $i = 30^\circ$, $a_{\rm crit}$ is mostly unchanged. Thus, the fit from HW99 has a similar level of agreement in these cases as it does in the coplanar cases. In about half of all cases, $a_{\rm st}$ remains the same as in the coplanar case. In the other half of cases, $a_{\rm st}$ increases to the next $n:1$ MMR. This creates a wider gap between $a_{\rm st}$ and $a_{\rm crit}$ on average.

the mutual inclination i and that this dependence is almost negligible for $i \lesssim 40^\circ$. This is especially true for $a_{\rm crit}$. Thus, for low-to-intermediate inclinations, the innermost stable circumbinary orbit is well characterized by the coplanar case, and therefore well described by the (coplanar) parametric fit of HW99 (within the error of the linear-regression fit). At higher inclinations ($i \gtrsim 40^\circ$), there is a weak an nearly monotonic dependence of $a_{\rm crit}$ on i for *fixed* $e_{\rm b}$ and $\mu_{\rm b}$; however, this trend can be decreasing or increasing for different combination of binary parameters. This is particularly evident in the circular binary case in Fig. 10, where $a_{\rm crit}$ grows with inclination for $\mu_{\rm b} = 0.1$, but decreases with i when $\mu_{\rm b} = 0.5$. Previous work by Doolin & Blundell (2011) shows consistent results with these non-trivial trends (see Section 4 below). The values of $a_{\rm st}$ show similar general trends for low and high inclinations. However, for i above $\sim 40^\circ$ the outlier outcomes described in Section 3.3 imply that for certain combinations of $e_{\rm b}$, $\mu_{\rm b}$ and i exhibit a distinct long-term behavior which does not change $a_{\rm crit}$, but that drastically modifies the values of $a_{\rm st}$. In Section 3.3, we have speculated that these unusual dynamics might be the result of long-term secular effects.

3.4.2 *Fitting formulae*

We present fits to $a_{\rm crit}$ and $a_{\rm st}$ as functions of mass ratio and eccentricity at different fixed inclinations. As the dependence of the critical boundaries on inclination is complex – even when monotonic in i for fixed $e_{\rm b}$, $\mu_{\rm b}$, the sign of the change can depend sensitively on the specific value of $e_{\rm b}$ and $\mu_{\rm b}$ – a global multi-dimensional fit for the three independent variables $e_{\rm b}$, $\mu_{\rm b}$ and i does not provide any useful insight. Instead, for *fixed* values of i we provide fits of the form

$$a_{\rm crit,st}(e_{\rm b},\mu_{\rm b};i) = A + Be_{\rm b} + Ce_{\rm b}^2 + D\mu_{\rm b} + Ee_{\rm b}\mu_{\rm b} + F\mu_{\rm b}^2 + Ge_{\rm b}^2\mu_{\rm b}^2 \quad (4)$$

obtained from least-squares fitting on six variables: $e_{\rm b}$, $e_{\rm b}^2$, $\mu_{\rm b}$, $\mu_{\rm b}^2$, $e_{\rm b}\mu_{\rm b}$ and $e_{\rm b}^2\mu_{\rm b}^2$ (HW99). As the outliers cases described in Section 3.3 complicate the dependence of $a_{\rm crit}$ and $a_{\rm st}$ on inclination even further, we do not attempt this parametric fit for $i \geqslant 40^\circ$.

Table 3 lists five set of 7 least-squares coefficients required to specify the fit for $a_{\rm crit}$ as in Eq. (4) for 5 different inclinations. Similarly, Table 4 lists the coefficients that specify the parametric fit for $a_{\rm st}$ for the same 5 inclinations. The two fits for $a_{\rm crit}$ and $a_{\rm st}$ in the coplanar case work equally well with average residuals of

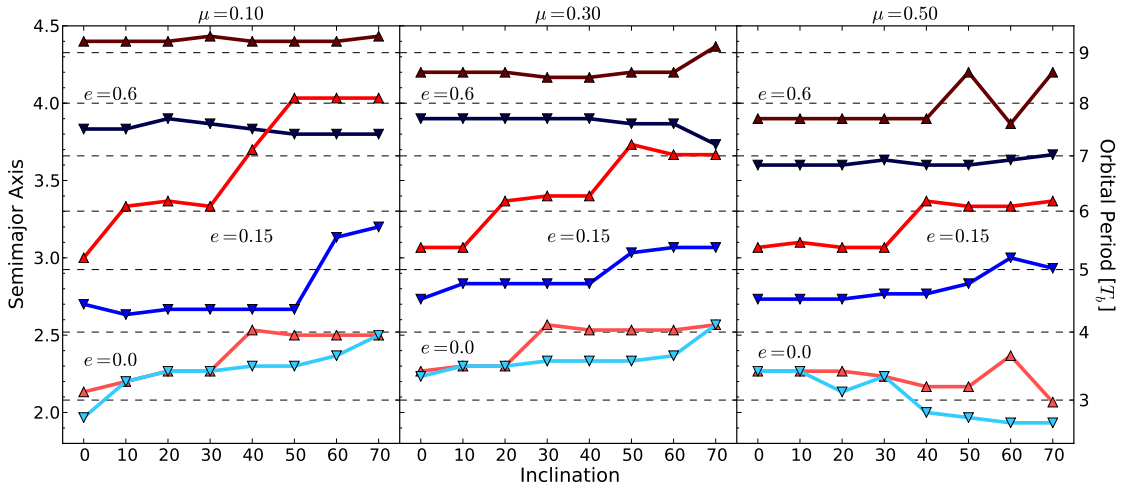

Figure 10. The dependences of $a_{\rm crit}$ and $a_{\rm st}$ on planetary inclination for binary mass ratios $\mu_{\rm b}$ of 0.1, 0.3, and 0.5, and eccentricities of 0.0, 0.15, and 0.6. In each pair of lines, the top redder line refers to $a_{\rm st}$ and the bottom blue line refers to $a_{\rm crit}$. For low eccentricities, $a_{\rm crit}$ and $a_{\rm st}$ are mostly unchanged at $i \leqslant 20°$. For $i \geqslant 30°$, $a_{\rm st}$ at each $\mu_{\rm b}$ increases by $\sim 0.3 a_{\rm b}$ except in the equal mass case. For high eccentricities, both $a_{\rm crit}$ and $a_{\rm st}$ are mostly constant across all prograde inclinations.

Table 3. Fitting Formulas for $a_{\rm crit}$ at Low Inclinations

i_0	const.	e	e^2	$\mu_{\rm b}$	$e\mu_{\rm b}$	$\mu_{\rm b}^2$	$e^2\mu_{\rm b}^2$
HW99	1.60 ± 0.04	5.10 ± 0.05	-2.22 ± 0.11	4.12 ± 0.09	-4.27 ± 0.17	-5.09 ± 0.11	4.61 ± 0.36
0°	1.66 ± 0.07	5.04 ± 0.26	-2.28 ± 0.25	3.15 ± 0.39	-2.72 ± 0.76	-4.16 ± 0.55	-0.03 ± 1.71
10°	1.79 ± 0.06	4.43 ± 0.23	-1.76 ± 0.22	2.88 ± 0.35	-1.47 ± 0.68	-4.02 ± 0.49	-2.94 ± 1.54
20°	1.92 ± 0.06	4.11 ± 0.23	-1.57 ± 0.22	2.34 ± 0.35	-0.66 ± 0.68	-3.37 ± 0.49	-4.23 ± 1.53
30°	2.04 ± 0.06	3.19 ± 0.23	-0.86 ± 0.22	2.43 ± 0.35	-1.14 ± 0.68	-4.06 ± 0.49	-7.00 ± 1.54
40°	2.23 ± 0.08	2.23 ± 0.30	0.06 ± 0.29	1.41 ± 0.46	3.41 ± 0.90	-2.78 ± 0.64	-12.27 ± 2.02

Each least-squares fit has the form of $a_{crit}(e, \mu_{\rm b}, i = i_0)$ = A +Be + Ce^2 + D$\mu_{\rm b}$ + E$e\mu_{\rm b}$ + F$\mu_{\rm b}^2$ +G$e^2\mu_{\rm b}^2$.
The fit from HW99 is given for comparison.

about 2% and maximum residuals 8%. For the inclined cases, the fits for $a_{\rm crit}$ work much better than those for $a_{\rm st}$ because the fits are unable to reproduce the step function nature of $a_{\rm st}$. Like the coplanar fit for $a_{\rm crit}$, the fits for $a$crit for the inclined orbits have residuals of about 2% with maxima of no more than 8%. Unlike the coplanar fit for $a_{\rm st}$, the fits for $a_{\rm st}$ for the inclined orbits have residuals of about 3% with maxima typically between 12 to 20%.

4 DISCUSSION

Parametrized stability boundaries provide a rapid assessment of the viability of specific orbital configurations (HW99; Mardling & Aarseth 1999; Petrovich 2015). In the context of circumbinary planets, these stability boundaries also inform us about constraint and obstacles to planet formation and planet migration. The *apparent* pile-up of planets near $a_{\rm crit}$ (e.g., Welsh et al. 2014) might indicate either a preferred planet formation site, or a location where planet migration stalls (e.g. Nelson 2003; Kley & Haghighipour 2014). In addition to the existence of $a_{\rm crit}$, the presence of multiple instability islands due to high-order MMRs with the central binary pose a (slower, long-term) threat to the stability of planets (e.g., Kostov et al. 2013; Popova & Shevchenko 2013), which indicates that the eccentricity damping that results from planet-disc interaction overcomes any resonant excitation and/or that migrating planets cross these islands too quickly for the resonance to matter.

The yet unclear nature of the protoplanetary gas discs that give birth to circumbinary planets justifies studying the associated stability boundaries under significant mutual inclinations. While some discs around close binaries seem to be well aligned with their hosts (Czekala et al. 2015, 2016), wider configurations (Brinch et al. 2016) do not appear to obey this constraint, nor have they had enough time to evolve into coplanarity (Foucart & Lai 2013). In addition, the possibility of external mechanisms being responsible for a slow misalignment of planets around the most compact binaries (Muñoz & Lai 2015) further support the need for updated stability criteria.

Our results confirm the previous numerical explorations of HW99 of circumbinary planet stability in coplanarity (Fig. 8). We further assess the ejection times associated with the inner boundary $a_{\rm crit}$ and the outer boundary $a_{\rm st}$; confirming that integration times of $10^4 T_b$ is roughly sufficient to confidently identify $a_{\rm crit}$, although much longer integration times are required to capture ejections at different high-order MMRs. The values of $a_{\rm crit}$ of HW99 are also valid (within the uncertainties of their parametric fit) for inclined planets when $i \lesssim 30°$. At higher inclinations, however, the evolution of both $a_{\rm crit}$ and $a_{\rm st}$ show a non-trivial dependence on i. We often find constant $a_{\rm crit}$ with i up to 20° or 40°, while fol-

Table 4. Fitting Formulas for $a_{\rm st}$ at Low Inclinations

i_0	const.	$e_{\rm b}$	$e_{\rm b}^2$	$\mu_{\rm b}$	$e_{\rm b}\mu_{\rm b}$	$\mu_{\rm b}^2$	$e^2\mu_{\rm b}^2$
0°	1.98 ± 0.09	6.45 ± 0.33	-3.93 ± 0.32	2.31 ± 0.50	-5.47 ± 0.98	-2.95 ± 0.70	6.22 ± 2.21
10°	2.43 ± 0.11	5.29 ± 0.42	-3.38 ± 0.40	0.94 ± 0.63	-2.47 ± 1.23	-1.74 ± 0.88	1.61 ± 2.78
20°	2.39 ± 0.11	5.43 ± 0.43	-3.60 ± 0.41	1.41 ± 0.65	-2.44 ± 1.28	-2.44 ± 0.92	1.60 ± 2.88
30°	2.54 ± 0.11	4.85 ± 0.42	-3.07 ± 0.40	0.90 ± 0.63	-1.21 ± 1.23	-1.81 ± 0.88	-0.96 ± 2.78
40°	2.85 ± 0.14	4.08 ± 0.53	-2.56 ± 0.50	0.30 ± 0.80	-0.22 ± 1.56	-1.65 ± 1.12	-1.31 ± 3.52

Each least-squares fit has the form of $a_{st}(e, \mu_{\rm b}, i = i_0)$ = A +Be + Ce^2 + D$\mu_{\rm b}$ + E$e\mu_{\rm b}$ + F$\mu_{\rm b}^2$ +G$e^2\mu_{\rm b}^2$.

lowed by an increase of the stability boundary of $i \gtrsim 40^\circ$. Some cases do not follow this trend. When $\mu_{\rm b} = 0.5$, for example, may exhibit entirely different trends (Fig. 10). These trends are also in agreement with the work of (Doolin & Blundell 2011), which is the most similar calculation to the one presented here (despite the differencein the choice of the initial planetary line of nodes; see Section 2.2.2 and Fig. 1). In the region of parameter space for which both works should be equivalent (planetary nodal circulation; red region in Fig. 1) we find qualitatively consistent results: $a_{\rm crit}$ shrinks with i for low $e_{\rm b}$ and $\mu_{\rm b} = 0.5$; $a_{\rm crit}$ grows with i for low $e_{\rm b}$ and $\mu_{\rm b} < 0.5$; $a_{\rm crit}$ is roughly indifferent to (or erratic with) i for $e_{\rm b} > 0.2$. Those authors do find significant stabilization for *retrograde* planetary orbits, a regime that we have not explored here. In regards to the values of $a_{\rm st}$ it is difficult to compare both studies, although the rough stability structure outside $a_{\rm crit}$ exhibits the same features. Interestingly, their integration time of only 5×10^4 $T_{\rm b}$ implies that – according to Fig. 5 – they should have missed islands of instability for 31% of the configurations in the mutually overlapping parameter space.

This general dependence on mutual inclination is in rough consistency with the results of triple system stability of (Petrovich 2015) (in a different mass regime), who found no effect of mutual inclination for $i \lesssim 20^\circ$, a slight stabilizing effect (closer orbits are possible) for $20^\circ \lesssim i \lesssim 40^\circ$, and a destabilizing effect for $i \gtrsim 40^\circ$. Interestingly, in the widely used triple system stability criterion of Mardling & Aarseth (1999) (yet for an entirely different mass regime) mutual inclination works always a stabilizing factor.

The last stable circular orbit bears some resemblance to the "truncation radius" of circumbinary discs (Artymowicz & Lubow 1994; Miranda & Lai 2015). The truncation of inclined discs obtained by Miranda & Lai (2015) *shrinks with* i, naively pointing toward inclination as responsible for increased stability. Nevertheless, that derivation is based upon finding on a balance between the disc's internal viscous torques with the external tidal torques exerted by the binary, which are indeed weakened by inclination. However, in N-body computations, there is no diffusive element, and although inclined tidal torques at a given radius might be weakened, this will, at most, delay ejection, but not prevent it.

5 SUMMARY AND CONCLUSIONS

We used numerical N-body integrations to analyze the stability of circumbinary planets for different combinations of binary parameters (eccentricity and mass ratio) and to provide parametric fits to critical stability boundaries in this type system. We characterize the inner limit of stability around a binary with a semi-major axis $a_{\rm crit}$ inside which all near circular orbits are unstable. Beyond this distance, additional unstable regions appear at islands centered on all n : 1 MMRs exterior to $a_{\rm crit}$. We find that each successive island has a thinner width and exponentially larger ejection timescale. Since the levels of instability quickly decay after just the first few islands, we are able to measure the outer boundary of the meta-stable region with a semi-major axis $a_{\rm st}$ that is typically located just outside an n : 1 MMR.

This work extends previous studies in two ways: (1) we consider a wide range of planetary inclinations (0° to 90°) and (2) we integrated over timescales of 3×10^5 and, in some cases, up to 10^9 times the binary orbital period $T_{\rm b}$. These integrations times are up to orders of magnitude longer than previous studies and have enable us to test probe the weakest mean motion resonances that produce ejections on very long timescales. In addition, these long integration times probe into orbital evolution of planetary orbits on secular timescales, which for inclined systems, can result in non-trivial behavior impossible to capture over shorter integration times. Finally, integration times of 10^9 binary orbits can represent a significant fraction of the true lifetime of the stellar binaries with physical semi-major axes of a fraction of 1 AU, such some of the close eclipsing binaries known to host planets in the *Kepler catalog* (for which $T_{\rm b} \sim 0.1$yr).

We have provided parametric fits to two main stability boundaries around eccentric binaries. Our main findings are:

- Orbital fits of HW99 are still largely valid in moderately inclined cases (up to $i \sim 30^\circ$, but at high inclinations, their applicability is diminished.
- Parametric fits to stability boundaries do not respond to inclination in a trivial/monotonic manner, and inclination does not necessarily act as a stabilizing agent (i.e., by reducing the critical radii $a_{\rm crit}$) as some stability criterion in the literature may imply.
- Our long integrations have allowed us to probe into the secular regime of orbital evolution. We have found a portion of parameter space that continuously degrades the stability of inclined circumbinary planets, moving the UCO boundary $a_{\rm crit}$ to wider orbits. We postulate that this effect is the result of an "external Kozai" effect, which only takes place when $\mu_b \neq 0.5$.

ACKNOWLEDGEMENTS

We thank Kaitlin Kratter for helpful discussions. This material is based upon work supported by the National Science Foundation under Grant No. 1228509. MH is supported by the NSF Graduate Research Fellowship under Grant No. DGE 1143953.

REFERENCES

Armstrong D. J., Osborn H. P., Brown D. J. A., Faedi F., Gómez

Maqueo Chew Y., Martin D. V., Pollacco D., Udry S., 2014, MNRAS, 444, 1873
Artymowicz P., Lubow S. H., 1994, ApJ, 421, 651
Borkovits T., Érdi B., Forgács-Dajka E., Kovács T., 2003, A & A, 398, 1091
Brinch C., Jørgensen J. K., Hogerheijde M. R., Nelson R. P., Gressel O., 2016, ApJ, 830, L16
Chambers J. E., 1999, MNRAS, 304, 793
Czekala I., Andrews S. M., Mandel K. S., Hogg D. W., Green G. M., 2015, ApJ, 812, 128
Czekala I., Andrews S. M., Torres G., Jensen E. L. N., Stassun K. G., Wilner D. J., Latham D. W., 2016, ApJ, 818, 156
Doolin S., Blundell K. M., 2011, MNRAS, 418, 2656
Doyle L. R., Carter J. A., Fabrycky D. C., Slawson R. W., Howell S. B., et al. 2011, Science, 333, 1602
Dvorak R., 1986, A & A, 167, 379
Dvorak R., Froeschle C., 1989, A & A, 226, 335
Farago F., Laskar J., 2010, MNRAS, 401, 1189
Foucart F., Lai D., 2013, ApJ, 764, 106
Fressin F., Torres G., Charbonneau D., Bryson S. T., Christiansen J., Dressing C. D., Jenkins J. M., Walkowicz L. M., Batalha N. M., 2013, ApJ, 766, 81
Gladman B., 1993, Icarus, 106, 247
Grishin E., Perets H. B., Zenati Y., Michaely E., 2016, ArXiv e-prints
Hamers A. S., Perets H. B., Portegies Zwart S. F., 2016, MNRAS, 455, 3180
Holman M. J., Wiegert P. A., 1999, AJ, 117, 621
Kley W., Haghighipour N., 2014, A & A, 564, A72
Kostov V. B., McCullough P. R., Carter J. A., Deleuil M., Díaz R. F., et al. 2014, ApJ, 784, 14
Kostov V. B., McCullough P. R., Hinse T. C., Tsvetanov Z. I., Hébrard G., et al. 2013, ApJ, 770, 52
Leung G. C. K., Lee M. H., 2013, ApJ, 763, 107
Liu B., Muñoz D. J., Lai D., 2015, MNRAS, 447, 747
Mardling R., Aarseth S., 1999, in Steves B. A., Roy A. E., eds, NATO Advanced Science Institutes (ASI) Series C Vol. 522 of NATO Advanced Science Institutes (ASI) Series C, Dynamics and Stability of Three-Body Systems. p. 385
Mardling R. A., Aarseth S. J., 2001, MNRAS, 321, 398
Martin D. V., Triaud A. H. M. J., 2014, A & A, 570, A91
Martin D. V., Triaud A. H. M. J., 2015, MNRAS, 449, 781
Miranda R., Lai D., 2015, MNRAS, 452, 2396
Moriwaki K., Nakagawa Y., 2004, ApJ, 609, 1065
Muñoz D. J., Lai D., 2015, Proceedings of the National Academy of Science, 112, 9264
Nelson R. P., 2003, MNRAS, 345, 233
Orosz J. A., Welsh W. F., Carter J. A., Fabrycky D. C., Cochran W. D., et al. 2012, Science, 337, 1511
Paardekooper S.-J., Leinhardt Z. M., Thébault P., Baruteau C., 2012, ApJ, 754, L16
Petrovich C., 2015, ApJ, 808, 120
Petrovich C., Muñoz D. J., 2016, ArXiv e-prints (arXiv:1607.0489)
Pichardo B., Sparke L. S., Aguilar L. A., 2005, MNRAS, 359, 521
Pilat-Lohinger E., Funk B., Dvorak R., 2003, A & A, 400, 1085
Popova E. A., Shevchenko I. I., 2013, ApJ, 769, 152
Press W. H., Flannery B. P., Teukolsky S. A., 1986, Numerical recipes. The art of scientific computing
Rafikov R. R., 2013, ApJ, 764, L16
Schneider J., 1994, Planet. Space Sci., 42, 539
Smullen R. A., Kratter K. M., Shannon A., 2016, MNRAS
Sutherland A. P., Fabrycky D. C., 2016, ApJ, 818, 6
Welsh W. F., Orosz J. A., Carter J. A., Fabrycky D. C., et al. 2014, in Haghighipour N., ed., IAU Symposium Vol. 293 of IAU Symposium, Recent Kepler Results On Circumbinary Planets. pp 125–132
Welsh W. F., Orosz J. A., Carter J. A., Fabrycky D. C., Ford E. B., et al. 2012, Nature, 481, 475
Wisdom J., 1980, AJ, 85, 1122
Youdin A. N., Kratter K. M., Kenyon S. J., 2012, ApJ, 755, 17